ACCEPTED VERSION

Laiquan Li, Hongbin Yang, Jianwei Miao, Liping Zhang, Hsin-Yi Wang, Zhiping Zeng, Wei Huang, Xiaochen Dong, and Bin Liu
Unraveling oxygen evolution reaction on carbon-based electrocatalysts: effect of oxygen doping on adsorption of oxygenated intermediates

---

Unraveling Oxygen Evolution Reaction on Carbon-Based Electrocatalysts: Effect of Oxygen Doping on Adsorption of Oxygenated Intermediates

Laiquan Li,[†,‡,§] Hongbin Yang,[†,§] Jianwei Miao,[†] Liping Zhang,[†] Hsin-Yi Wang,[†] Zhiping Zeng,[†] Wei Huang,[‡●] Xiaochen Dong,*[‡] and Bin Liu*[†●]

[†]School of Chemical and Biomedical Engineering, Nanyang Technological University, 62 Nanyang Drive, Singapore 637459, Singapore

[‡]Key Laboratory of Flexible Electronics (KLOFE) & Institute of Advanced Materials (IAM), Jiangsu National Synergistic Innovation Center for Advanced Materials (SICAM), Nanjing Tech University (NanjingTech), 30 South Puzhu Road, Nanjing 211816, China

S *Supporting Information*

ABSTRACT: Carbon-based nanomaterials have been widely studied as promising electrocatalysts for energy conversion and storage. Understanding the oxygen evolution and reduction reactions on carbon-based nanomaterials is of critical importance for development of highly active metal-free electrocatalysts. Here, the adsorption of oxygenated intermediates during oxygen evolution reaction (OER) on carbon nanotubes (CNTs) was examined by ex-situ X-ray photoelectron spectroscopy and in situ electrochemical impedance spectroscopy. The results demonstrate that the carbon atoms on CNTs near the C=O functional groups are active for OER. On the basis of this result, we further revealed the origin of the enhanced intermediate adsorption on surface-oxidized CNTs and the relationship between surface groups and apparent activation energy. Our study gained new understanding of OER on oxygen-doped carbon nanomaterials and provided an effective approach for investigating electrocatalysis on heteroatom-doped carbon electrocatalysts.
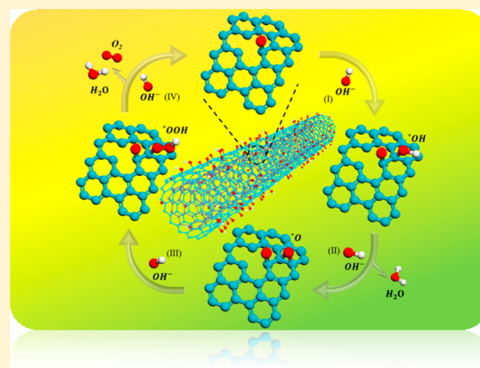
Electrocatalysis plays a vital role in electrochemical energy conversion and storage, e.g., water splitting, metal–air batteries, and fuel cells.[1–4] Carbon nanomaterials with multidimensional nanoarchitecture and tunable electronic and surface properties have been extensively investigated.[5–8] Many methods for nanoarchitecture engineering of carbon nanomaterials have been developed toward oxygen evolution reaction (OER) and oxygen reduction reaction (ORR), including surface functionalization[9–11] and heteroatom doping, such as nitrogen,[12–14] boron,[15,16] oxygen,[17,18] or sulfur.[19,20] Both incorporation of functional groups and heteroatoms in carbon network change the electronic properties of their peripheral carbon atoms, which in turn affect their electrocatalytic performance. Unfortunately, it remains difficult to understand OER and ORR mechanisms on carbon materials because of the diverse functional groups, complicated dopant locations, and multifarious surface states.[21,22] In the field of electrocatalysis, electrochemical processes generally take place at the interface between electrode and electrolyte.[23] Therefore, investigating the physical and chemical processes at the electrode–

electrolyte interface is vitally important to understand the related reactions and mechanisms. It is generally accepted that the formation of adsorbed intermediates determines the catalyst performance.[2,24] Therefore, detection of reaction intermediates could provide a direct way to identify catalytic active sites and reaction pathways.

Herein, we chose carbon nanotubes (CNTs) as a model system to study OER in alkaline media. The influence of oxygen functional groups, which was tuned by oxygen plasma oxidation and/or thermal reduction, on adsorption of reaction intermediates was systemically investigated by ex situ X-ray photoelectron spectroscopy (XPS) and in situ electrochemical impedance spectroscopy (EIS). For the first time, the oxygenated intermediates were experimentally identified at CNTs surface during OER: the C=O group was found to play a crucial role in enhancing adsorption of reaction intermediates
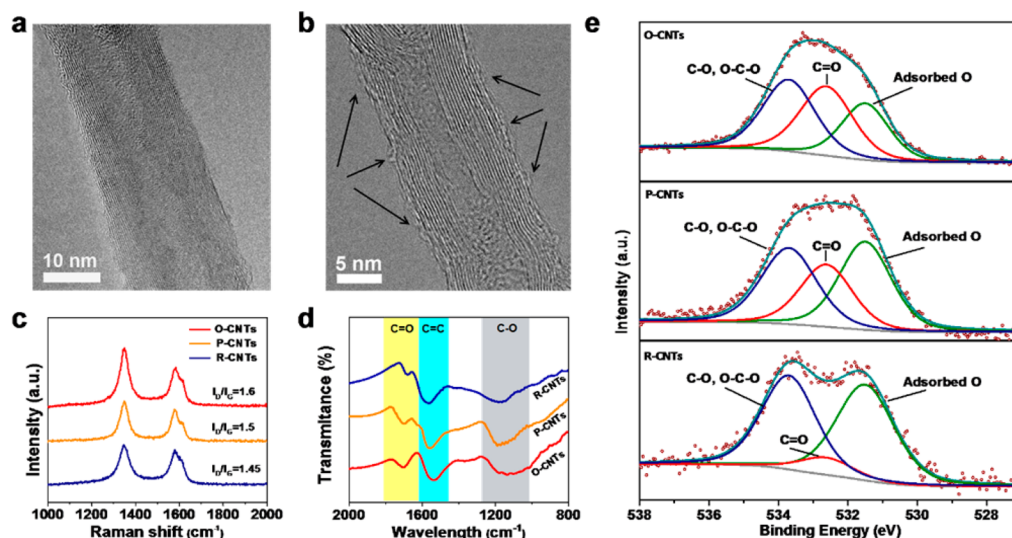
Figure 1. Physical characterizations of CNTs: (a) high-resolution TEM image of P-CNTs and (b) O-CNTs, (c) Raman spectra, (d) Fourier transform infrared spectroscopy (FTIR) spectra, and (e) deconvolution of the XPS O 1s spectra.

on its neighboring carbon atoms, which were identified as the active sites for OER. Our oxygen monodoped CNT catalyst could deliver an OER current density of 10 mA/cm^2 at an overpotential of 360 mV and remained stable over 24 h of continuous operation, which is much better than other heteroatom-doped CNTs.

The oxygen functional groups on CNTs were tuned by oxygen plasma oxidation (O-CNTs) or thermal reduction (R-CNTs). Figure 1a,b shows the TEM images of CNTs before and after O$_2$ plasma treatment. Compared to the pristine CNTs (P-CNTs), the rough surface of O-CNTs indicated that the outer-surface of P-CNTs was mildly etched by oxygen active species during O$_2$ plasma treatment, creating defects on the surface of O-CNTs. It is noteworthy that the plasma reactor used in this work has a maximum RF power of only 18 W, which is much weaker than the power used in conventional CNT O$_2$-plasma modification,[25−27] leading to a mild surface functionalization without dramatic structural damage. The carbon nanotube was paved into an ultrathin layer to homogeneously expose it to O$_2$ plasma (Figure S1). Figure 1c shows the Raman spectra of P-CNTs, R-CNTs, and O-CNTs. The intensity ratio of D-band to G-band (I_D/I_G) decreased from 1.5 to 1.45 from P-CNTs to R-CNTs. O$_2$ plasma treatment increased I_D/I_G only slightly to 1.6. These results suggest that O$_2$ plasma oxidation or thermal reduction exerts little influence on the bulk crystallinity of CNTs. Figure 1d displays the Fourier transform infrared spectroscopy (FTIR) spectra. The fraction of C=O stretching at around 1710 cm^{-1} gradually increases with different treatments from R-CNTs to O-CNTs.[28] The oxygen functional groups on the surface of CNTs were further analyzed by high-resolution O 1s XPS spectra, as displayed in Figure 1e. The spectrum could be deconvoluted into three peaks, which are assigned to C−O (C−O and C−O−C, 533.8 ± 0.2 eV), C=O (532.5 ± 0.2 eV), and physically adsorbed oxygen/carbonate species (531.3 ± 0.2 eV).[29] The oxygen atomic ratio for O-CNTs, P-CNTs, and R-CNTs were determined to be 8.2%, 7.2%, and 2.5%, respectively (Figure S3 and Table S1). Quantitative analysis shows that the atomic ratio of C=O was significantly increased from 1.9% to 3.1 atom % while the fraction of C−O remained almost unchanged (2.5 atom % for P-CNTs and 2.6 atom % for

O-CNTs) before and after O$_2$ plasma treatment (Tables S1 and S2). On the other hand, significant removal of the oxygen functional groups was achieved by thermal reduction in Ar/H$_2$ atmosphere; the atomic ratios of C−O and C=O in R-CNTs were reduced to 1.1% and 0.2 atom %, respectively, which is much lower than those in O-CNTs. The lower content of C=O as compared to C−O in R-CNTs is attributed to the inferior thermal stability of C=O.[30] Therefore, O$_2$ plasma treatment and/or thermal reduction can effectively tune the concentration of C−O and C=O functional groups on the surface of CNTs, rendering CNTs with different electronic properties, which in turn is expected to influence their electrocatalytic activities.

To reveal the variation of surface composition during OER and provide mechanistic information related to the adsorption of intermediates on CNTs, ex situ XPS and in situ EIS measurements were conducted. Figure 2a shows C 1s spectra of O-CNTs acquired after applying different anodic potentials for 15 min. At 1.2 V versus reversible hydrogen electrode (vs
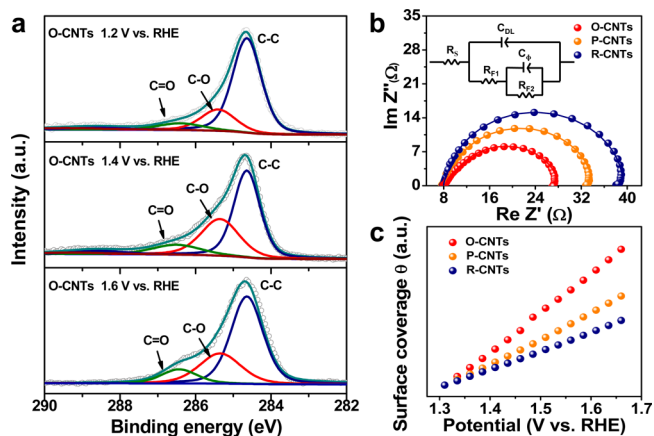

Figure 2. Ex situ XPS and in situ EIS measurements: (a) ex situ C 1s XPS spectra of O-CNTs acquired after applying anodic potentials for 15 min; (b) Nyquist plots of O-CNTs, P-CNTs, and R-CNTs obtained at 1.625 V vs RHE (inset, electrical equivalent circuit); and (c) variation in the surface coverage of intermediates on CNTs.
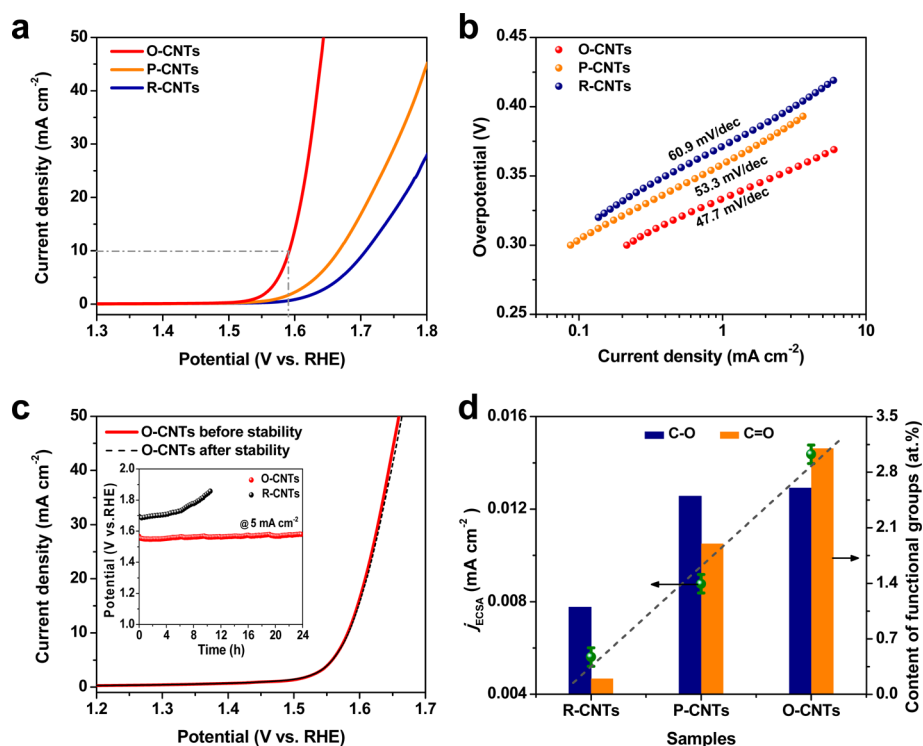
Figure 3. OER performances in 1 M KOH. (a) Linear sweep voltammetry (LSV) curves. (b) Tafel plots. (c) LSV curves for O-CNTs before and after long-term stability test. The inset shows the chronoamperometric responses for OER at current density of 5 mA cm^{-2}. (d) Comparison of OER current density (normalized with ECSA) at η = 300 mV with content of oxygen functional groups on different CNTs.

RHE) (below the thermodynamic potential for water oxidation), the recorded current is mainly contributed from the double-layer capacitance. Faradaic adsorption of oxygenated intermediates starts at higher applied potentials (e.g., 1.4 V vs RHE), while both intermediate adsorption and their conversion into molecular oxygen take place when the applied potential is further increased to 1.6 V vs RHE. The C 1s spectra were deconvoluted into three peaks: C–C (284.6 eV), C–O (285.4 eV), and C=O (286.5 eV).[28,31,32] Corresponding percentages of functional groups are summarized in Table S3. The C–O fraction can be assigned to the original C–O group on CNTs as well as the C-adsorbates bonding (C–OH*, C–O*, or C–OOH*). The peak intensity related to C–O increased from 18.4% at 1.2 V vs RHE to 31.4% at 1.4 V vs RHE, demonstrating an accumulation of intermediates on O-CNTs with increasing applied bias prior to the onset of OER. Further increase in applied bias slightly reduced the C–O content, which is likely due to the rapid consumption of intermediates for oxygen evolution. In contrast, no obvious variation of C–O content was noticed on R-CNTs with changing of applied biases (Figure S4 and Table S3), indicating very weak intermediate adsorption.

The in situ EIS analyses in the potential range from 1.35 to 1.65 V were conducted to further verify the enhanced intermediate adsorption on the oxygen-doped CNTs (Figure S5). Figure 2b compares experimental and simulated Nyquist plots obtained at an applied bias of 1.625 V. The inset of Figure 2b shows the electrical equivalent circuit used to simulate the electrode process.[33,34] R_S refers to the equivalent series resistance. The C_{DL} element models the double-layer capacitance. R_1 and R_2 determine the overall charge-transfer resistance (R_{CT}).[24,35] O-CNTs shows the smallest R_{CT}, indicating favorable OER kinetics. The surface intermediate

coverage (θ) can be estimated by the capacitance associated with intermediate adsorption ,C_ϕ,[36] which is defined as the derivative of intermediate coverage (θ) with potential:[24,37]

$$C_\phi(E) = \sigma(\mathrm{d}\theta(E)/\mathrm{d}E) \tag{1}$$

where σ is the charge density for a monolayer coverage (assumed to be constant). C_ϕ was obtained from the impedance spectroscopy and has been normalized to the electrocatalytically active surface area (Figures S5d and S6). Therefore, the surface intermediate coverage (θ) can be estimated by integrating C_ϕ with increasing applied potential, E.[24] As shown in Figure 2c, O-CNTs possess the largest surface intermediate coverage. These results are the first time the enhanced oxygenated intermediate adsorption on surface-oxidized CNTs was experimentally witnessed and verified by combining ex situ XPS observation with in situ EIS measurement.

The higher intermediate coverage on O-CNTs can originate from either stronger intermediate adsorption per active site or higher density of active sites. To reveal the active sites, OER activities of O-CNTs, P-CNTs, and R-CNTs were tested on a rotating disk electrode (RDE) in 1 and 0.1 M KOH (Figure S7). O-CNTs exhibited the best OER activity with the smallest onset overpotential of 290 mV and fastest elevating OER current, as shown in Figure 3a. The overpotential required to drive a current density of 10 mA cm^{-2} for O-CNTs is around 360 mV, significantly lower than that for P-CNTs and R-CNTs (450 and 530 mV) and other reported carbon-based electrocatalysts (Table S4). Rotating ring disk electrode (RRDE) measurements demonstrated negligible HO$_2^-$ formation and a 4-electron transfer process for OER on O-CNTs (Figure S8). Figure 3b shows the Tafel plots measured at 1 mV s^{-1} in 1 M KOH. O-CNTs possess the smallest Tafel slope of 47.7

mV dec^{-1} compared to P-CNTs (53.3 mV dec^{-1}) and R-CNTs (60.9 mV dec^{-1}). Long-term electrochemical stability was tested at a current density of 5 mA cm^{-2} (Figure 3c and inset). The O-CNTs exhibited much better stability with negligible performance degradation over 24 h of continuous operation, while the inferior stability of R-CNTs could be attributed to the sluggish kinetics of OER, leading to oxidation and decomposition of carbon during the OER process. Faradaic efficiency measurement revealed a nearly 100% efficiency toward oxygen evolution (Figure S9).

Figure 3d displays the correlation between OER current density (normalized with ECSA) at η = 300 mV and the atomic content of oxygen functional groups. With similar surface concentration of C−O, O-CNTs exhibited an OER current density much higher than that of P-CNTs. Interestingly, we found that the OER current density showed positive correlation with the content of C=O group for three CNT samples, indicating that C=O is predominantly responsible for the OER performance. Similar dependency between OER current density and content of C=O group at other potentials (1.52 and 1.54 V) in the kinetics control region further supported this conclusion (Figure S10). The influence of C=O on OER was further confirmed by measuring the OER current on reduced O-CNTs (RO-CNTs), which showed significantly diminished OER performance (Figure S11). Here it is necessary to highlight that the enhanced electrocatalytic performance induced by oxygen doping is not restricted to CNTs but is general to other carbon materials, e.g., carbon fibers and carbon black (Figure S12).

Recent DFT calculations on heteroatom-doped carbon materials have demonstrated that the carbon atoms next to the dopants generally serve as the active sites in electrocatalysis due to the doping-induced charge redistribution in the π-conjugated system.[13,38] In particular, an electron-withdrawing group can accept electrons from its adjacent carbon atoms, endowing them with p-type characteristics.[17,39] Therefore, we deduce that the main active sites for OER on oxygen-doped carbon materials originate from the carbon atoms near the C=O group. Highly electronegative oxygen atoms could induce positive charges on its adjacent carbon atoms, facilitating adsorption of key intermediates during OER. As deduced from the Tafel slope, the OER performance on CNTs was rate-determined at step II, that is, transition from C−OH* to C−O* (refer to the Supporting Information for detailed calculations). Therefore, a possible reaction pathway is proposed in Scheme 1 to explain the effect of oxygen doping on OER. The p-type domains of carbon atoms near the C=O group can easily accept electrons from OH$^-$ to form *OH (step I). Then the adsorbed *OH reacts with another OH$^-$ in solution to form *O; as mentioned above, this reaction is slow, which determines the overall rate of OER. This step can easily occur only in the presence of a C=O group, as its strong electron-withdrawing capability can induce positive charges on the adsorption sites and effectively reduce the energy barrier for the second OH$^-$ adsorption, thus triggering the transformation from *OH to *O (step II). Subsequently, *OOH will form from *O on the active sites by adsorbing another OH$^-$ (step III), followed by the release of molecular oxygen (step IV).

To further estimate the kinetical energy barrier involved in OER, the effect of temperature on OER performance was investigated (Figures 4, S13, and S14). With increasing temperature, both O-CNTs and R-CNTs exhibited improved OER performance with reduced onset potential (Figure 4a,b)

Scheme 1. Proposed OER Pathway on O-CNTs
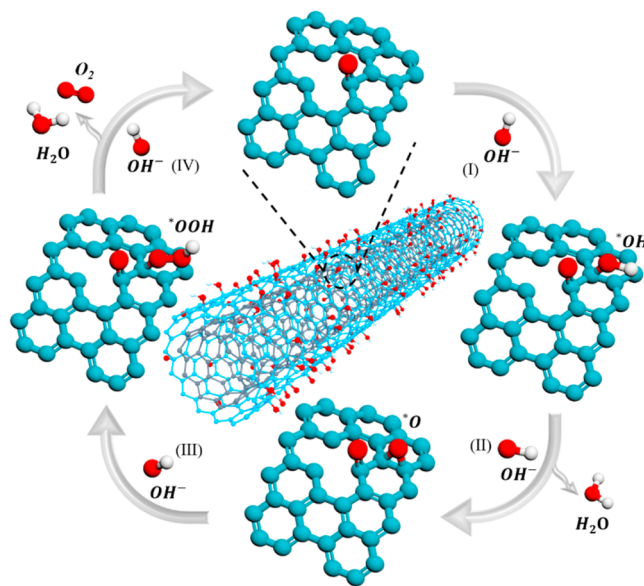
and slight decrease in Tafel slope (Figure S13), indicating a similar reaction mechanism on O-CNTs and R-CNTs. Furthermore, turnover frequency (TOF) calculations (Supporting Information) revealed similar values for O-CNTs and R-CNTs, indicative of the same type of active site. The reaction activation energy was extracted from the Arrhenius plots:[40,41]

$$\frac{d\ln(i)}{d(1/T)} = -\frac{E_{a,app}}{R} \tag{2}$$

where $E_{a,app}$ is the apparent activation energy, R the gas constant, and T the absolute temperature in Kelvin.

From the Arrhenius plot as shown in Figure 4c, the $E_{a,app}$ of O-CNTs was estimated to be ~31.5 kJ mol^{-1}, much smaller than that of R-CNTs (~52.6 kJ mol^{-1}), implying different OER thermodynamics, even though O-CNTs and R-CNTs share the same type of active sites. The effect of temperature on OER and distinguished $E_{a,app}$ of O-CNTs and R-CNTs are illustrated in Figure 4d. In general, reactants require enough kinetic energy to overcome the energy barrier to form products. Higher temperature results in stronger kinetic energy, which can provide more "qualified" reactants, manifesting a decrease in OER onset potential (Figure 4a,b). The activation energy (E_a) refers to the energy difference between reactants and the activated complex, also known as the transition state. As discussed above, the carbon atoms near C=O are active for OER, but because of different concentrations of C=O and complex surface environments, carbon atoms near C=O in O-CNTs and R-CNTs could possess a distribution of catalytic activities (representing the transition states with different energy levels). O-CNTs have higher density of active sites and thus possess higher density of state at the same energy level as compared to R-CNTs (inset in Figure 4d). During OER, active sites with higher catalytic activity (smaller activation energy) will be first occupied by reactants. Therefore, at a certain reaction temperature, it is easier for reactants to be driven toward the transition state on a catalyst with a deeper DOS distribution. Thus, O-CNTs has an $E_{a,app}$ that is lower than that of R-CNTs.

In summary, we used a combination of ex-situ XPS and in situ EIS techniques to experimentally identify enhanced
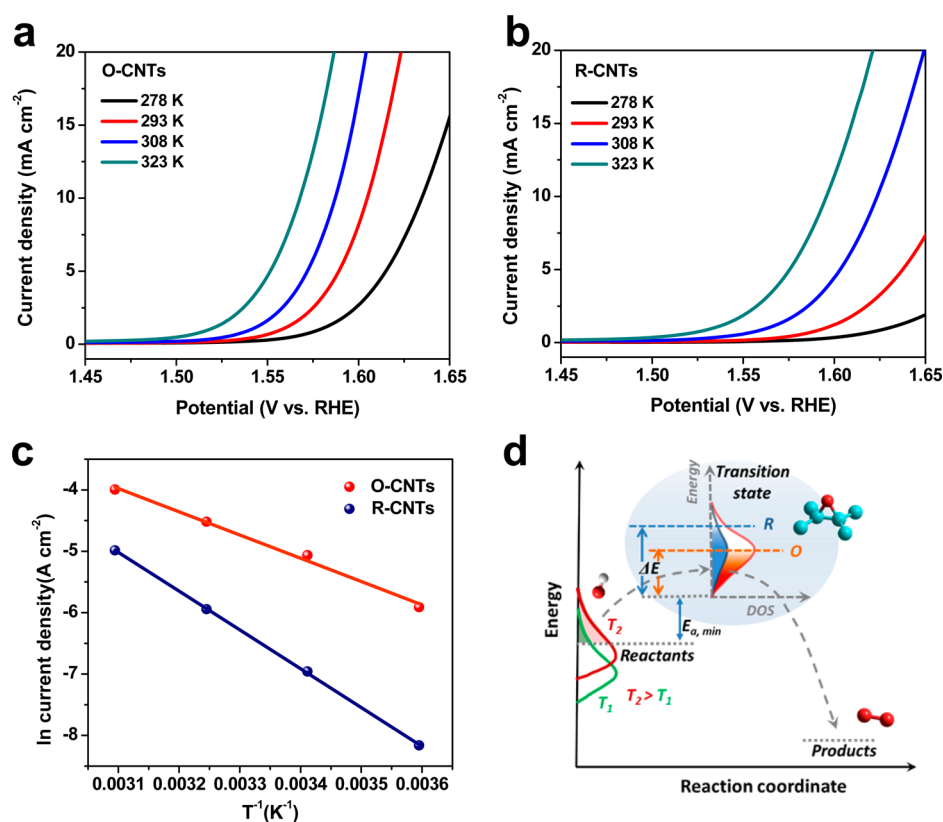
Figure 4. OER polarization curves of (a) O-CNTs and (b) R-CNTs acquired in 1 M KOH aqueous electrolyte with a scan rate of 1 mV s^{-1} at 5, 20, 35, and 50 °C. (Note that the variation of pH value and reference potential caused by the increasing temperature has been normalized). (c) Arrhenius plots acquired at an overpotential of 360 mV. (d) Energetic illustration of the OER process on CNTs. Inset (the part with light blue background) shows the energy and density of state (DOS) related transition states of the OER process on O-CNTs and R-CNTs. $E_{a,min}$ is the minimum activation energy; ΔE is the activation energy variation resulting from catalytic activity distribution of active sites. $E_{a,app} = E_{a,min} + \Delta E$. DOS represents the density of active sites with certain activation energy ($E_{a,min} + \Delta E$), and R and O refer to R-CNTs and O-CNTs, respectively.

adsorption of water oxidation intermediates on surface oxidized CNTs. The C=O functional group on CNTs was found to play a crucial role in altering the electronic cloud around the adjacent carbon atoms and thus facilitating the adsorption of oxygenated intermediates. On the basis of this result, we further revealed the origin of the enhanced intermediate adsorption on surface oxidized CNTs and the relationship with apparent activation energy. Our work provided a general understanding of OER electrocatalysis on oxygen-doped carbon nanomaterials and could open up new directions for design of superior carbon-based electrocatalysts.

■ ASSOCIATED CONTENT

ⓢ Supporting Information

The Supporting Information is available free of charge on the ACS Publications website at DOI: 10.1021/acsenergy-lett.6b00681.

    Experimental Section and supplementary figures and tables as discussed in the text (PDF)

■ AUTHOR INFORMATION

Corresponding Authors

*E-mail: iamxcdong@njtech.edu.cn.
*E-mail: liubin@ntu.edu.sg.

ORCID ⓘ

Wei Huang: 0000-0001-7004-6408

Bin Liu: 0000-0002-4685-2052

Author Contributions

§L.L. and H.Y. contributed equally to this work.

Notes

The authors declare no competing financial interest.

■ ACKNOWLEDGMENTS

■ REFERENCES

(1) Schlogl, R. The Role of Chemistry in the Energy Challenge. *ChemSusChem* **2010**, *3*, 209−222.

(2) Katsounaros, I.; Cherevko, S.; Zeradjanin, A. R.; Mayrhofer, K. J. J. Oxygen Electrochemistry as a Cornerstone for Sustainable Energy Conversion. *Angew. Chem., Int. Ed.* **2014**, *53*, 102−121.

(3) Liang, Y. Y.; Li, Y. G.; Wang, H. L.; Zhou, J. G.; Wang, J.; Regier, T.; Dai, H. J. Co$_3$O$_4$ Nanocrystals on Graphene as a Synergistic Catalyst for Oxygen Reduction Reaction. *Nat. Mater.* **2011**, *10*, 780–786.

(4) Zhang, J. T.; Zhao, Z. H.; Xia, Z. H.; Dai, L. M. A Metal-free Bifunctional Electrocatalyst for Oxygen Reduction and Oxygen Evolution Reactions. *Nat. Nanotechnol.* **2015**, *10*, 444–452.

(5) Zhang, J. T.; Xia, Z. H.; Dai, L. M. Carbon-based Electrocatalysts for Advanced Energy Conversion and Storage. *Sci. Adv.* **2015**, *1*, e1500564.

(6) Wu, G.; Mack, N. H.; Gao, W.; Ma, S. G.; Zhong, R. Q.; Han, J. T.; Baldwin, J. K.; Zelenay, P. Nitrogen-Doped Graphene-Rich Catalysts Derived from Heteroatom Polymers for Oxygen Reduction in Nonaqueous Lithium-O$_2$ Battery Cathodes. *ACS Nano* **2012**, *6*, 9764–9776.

(7) Li, Q.; Cao, R.; Cho, J.; Wu, G. Nanocarbon Electrocatalysts for Oxygen Reduction in Alkaline Media for Advanced Energy Conversion and Storage. *Adv. Energy Mater.* **2014**, *4*, 1301415.

(8) Ai, W.; Du, Z. Z.; Fan, Z. X.; Jiang, J.; Wang, Y. L.; Zhang, H.; Xie, L. H.; Huang, W.; Yu, T. Chemically Engineered Graphene Oxide as High Performance Cathode Materials for Li-ion Batteries. *Carbon* **2014**, *76*, 148–154.

(9) Dai, L. M. Functionalization of Graphene for Efficient Energy Conversion and Storage. *Acc. Chem. Res.* **2013**, *46*, 31–42.

(10) Wang, S. Y.; Yu, D. S.; Dai, L. M. Polyelectrolyte Functionalized Carbon Nanotubes as Efficient Metal-free Electrocatalysts for Oxygen Reduction. *J. Am. Chem. Soc.* **2011**, *133*, 5182–5185.

(11) Ma, T. Y.; Dai, S.; Jaroniec, M.; Qiao, S. Z. Graphitic Carbon Nitride Nanosheet-Carbon Nanotube Three-Dimensional Porous Composites as High-Performance Oxygen Evolution Electrocatalysts. *Angew. Chem., Int. Ed.* **2014**, *53*, 7281–7285.

(12) Chen, Z.; Higgins, D.; Chen, Z. W. Nitrogen Doped Carbon Nanotubes and Their Impact on the Oxygen Reduction Reaction in Fuel Cells. *Carbon* **2010**, *48*, 3057–3065.

(13) Guo, D. H.; Shibuya, R.; Akiba, C.; Saji, S.; Kondo, T.; Nakamura, J. Active Sites of Nitrogen-doped Carbon Materials for Oxygen Reduction Reaction Clarified Using Model Catalysts. *Science* **2016**, *351*, 361–365.

(14) Zhao, Y.; Nakamura, R.; Kamiya, K.; Nakanishi, S.; Hashimoto, K. Nitrogen-doped Carbon Nanomaterials as Non-metal Electrocatalysts for Water Oxidation. *Nat. Commun.* **2013**, *4*, 2390.

(15) Cheng, Y. H.; Tian, Y. Y.; Fan, X. Z.; Liu, J. G.; Yan, C. W. Boron Doped Multi-walled Carbon Nanotubes as Catalysts for Oxygen Reduction Reaction and Oxygen Evolution Reactionin in Alkaline Media. *Electrochim. Acta* **2014**, *143*, 291–296.

(16) Yang, L. J.; Jiang, S. J.; Zhao, Y.; Zhu, L.; Chen, S.; Wang, X. Z.; Wu, Q.; Ma, J.; Ma, Y. W.; Hu, Z. Boron-doped Carbon Nanotubes as Metal-free Electrocatalysts for the Oxygen Reduction Reaction. *Angew. Chem., Int. Ed.* **2011**, *50*, 7132–7135.

(17) Lu, X. Y.; Yim, W. L.; Suryanto, B. H. R.; Zhao, C. Electrocatalytic Oxygen Evolution at Surface-Oxidized Multiwall Carbon Nanotubes. *J. Am. Chem. Soc.* **2015**, *137*, 2901–2907.

(18) Silva, R.; Voiry, D.; Chhowalla, M.; Asefa, T. Efficient Metal-Free Electrocatalysts for Oxygen Reduction: Polyaniline-Derived N- and O-Doped Mesoporous Carbons. *J. Am. Chem. Soc.* **2013**, *135*, 7823–7826.

(19) Yu, X. W.; Zhang, M.; Chen, J.; Li, Y. R.; Shi, G. Q. Nitrogen and Sulfur Codoped Graphite Foam as a Self-Supported Metal-Free Electrocatalytic Electrode for Water Oxidation. *Adv. Energy Mater.* **2016**, *6*, 1501492.

(20) El-Sawy, A. M.; Mosa, I. M.; Su, D.; Guild, C. J.; Khalid, S.; Joesten, R.; Rusling, J. F.; Suib, S. L. Controlling the Active Sites of Sulfur-Doped Carbon Nanotube–Graphene Nanolobes for Highly Efficient Oxygen Evolution and Reduction Catalysis. *Adv. Energy Mater.* **2016**, *6*, 1501966.

(21) Navalon, S.; Dhakshinamoorthy, A.; Alvaro, M.; Garcia, H. Carbocatalysis by Graphene-Based Materials. *Chem. Rev.* **2014**, *114*, 6179–6212.

(22) Yan, Y. B.; Miao, J. W.; Yang, Z. H.; Xiao, F. X.; Yang, H. B.; Liu, B.; Yang, Y. H. Carbon Nanotube Catalysts: Recent Advances in Synthesis, Characterization and Applications. *Chem. Soc. Rev.* **2015**, *44*, 3295–3346.

(23) Strasser, P.; Ogasawara, H. In *Chemical Bonding at Surfaces and Interfaces*; Nilsson, A., Pettersson, L. G. M., Nørskov, J. K., Eds.; Elsevier: Amsterdam, 2008; pp 397–418.

(24) Tao, H. B.; Fang, L. W.; Chen, J. Z.; Yang, H. B.; Gao, J. J.; Miao, J. W.; Chen, S. L.; Liu, B. Identification of Surface Reactivity Descriptor for Transition Metal Oxides in Oxygen Evolution Reaction. *J. Am. Chem. Soc.* **2016**, *138*, 9978–9985.

(25) Chen, C. L.; Liang, B.; Ogino, A.; Wang, X. K.; Nagatsu, M. Oxygen Functionalization of Multiwall Carbon Nanotubes by Microwave-Excited Surface-Wave Plasma Treatment. *J. Phys. Chem. C* **2009**, *113*, 7659–7665.

(26) Tsai, W. L.; Huang, B. T.; Yang, P. Y.; Wang, K. Y.; Hsiao, C.; Cheng, H. C. Oxygen Plasma Functionalized Multiwalled Carbon Nanotube Thin Film as A pH Sensing Membrane of Extended-Gate Field-Effect Transistor. *IEEE Electron Device Lett.* **2013**, *34*, 1307–1309.

(27) Lobo, A. O.; Ramos, S. C.; Antunes, E. F.; Marciano, F. R.; Trava-Airoldi, V. J.; Corat, E. J. Fast Functionalization of Vertically Aligned Multiwalled Carbon Nanotubes Using Oxygen Plasma. *Mater. Lett.* **2012**, *70*, 89–93.

(28) Si, Y.; Samulski, E. T. Synthesis of Water Soluble Graphene. *Nano Lett.* **2008**, *8*, 1679–1682.

(29) Datsyuk, V.; Kalyva, M.; Papagelis, K.; Parthenios, J.; Tasis, D.; Siokou, A.; Kallitsis, I.; Galiotis, C. Chemical oxidation of multiwalled carbon nanotubes. *Carbon* **2008**, *46*, 833–840.

(30) Ganguly, A.; Sharma, S.; Papakonstantinou, P.; Hamilton, J. Probing the Thermal Deoxygenation of Graphene Oxide Using High-Resolution In Situ X-ray-Based Spectroscopies. *J. Phys. Chem. C* **2011**, *115*, 17009–17019.

(31) Okpalugo, T. I. T.; Papakonstantinou, P.; Murphy, H.; McLaughlin, J.; Brown, N. M. D. High Resolution XPS Characterization of Chemical Functionalised MWCNTs and SWCNTs. *Carbon* **2005**, *43*, 153–161.

(32) Yu, C.; Yang, J.; Zhao, C. T.; Fan, X. M.; Wang, G.; Qiu, J. S. Nanohybrids from NiCoAl-LDH Coupled with Carbon for Pseudocapacitors: Understanding the Role of Nano-structured Carbon. *Nanoscale* **2014**, *6*, 3097–3104.

(33) Conway, B. E. In *Impedance Spectroscopy: Theory, Experiment, and Application*, 2nd ed.; Macdonald, J. R., Barsoukov, E., Eds.; John Wiley & Sons, Inc.: Hoboken, NJ, 2005; pp 469–497.

(34) Lyons, M. E. G.; Brandon, M. P. The significance of electrochemical impedance spectra recorded during active oxygen evolution for oxide covered Ni, Co and Fe electrodes in alkaline solution. *J. Electoanal. Chem.* **2009**, *631*, 62–70.

(35) Doyle, R. L.; Lyons, M. E. G. An electrochemical impedance study of the oxygen evolution reaction at hydrous iron oxide in base. *Phys. Chem. Chem. Phys.* **2013**, *15*, 5224–5237.

(36) Harrington, D. A.; Conway, B. E. ac Impedance of Faradaic reactions involving electrosorbed intermediates—I. Kinetic theory. *Electrochim. Acta* **1987**, *32*, 1703–1712.

(37) Harrington, D. A.; Conway, B. E. Kinetic Theory of the Open-circuit Potential Decay Method for Evaluation of Behaviour of Adsorbed Intermediates: Analysis for the Case of the H$_2$ Evolution Reaction. *J. Electroanal. Chem. Interfacial Electrochem.* **1987**, *221*, 1–21.

(38) Jiao, Y.; Zheng, Y.; Davey, K.; Qiao, S.-Z. Activity Origin and Catalyst Design Principles for Electrocatalytic Hydrogen Evolution on Heteroatom-doped Graphene. *Nature Energy* **2016**, *1*, 16130.

(39) Yang, H. B.; Miao, J. W.; Hung, S.-F.; Chen, J. Z.; Tao, H. B.; Wang, X. Y.; Zhang, L. P.; Chen, R.; Gao, J. J.; Chen, H. M.; et al. Identification of Catalytic Sites for Oxygen Reduction and Oxygen Evolution in N-doped Graphene Materials: Development of Highly Efficient Metal-free Bifunctional Electrocatalyst. *Sci. Adv.* **2016**, *2*, e1501122.

(40) Zhang, B.; Zheng, X. L.; Voznyy, O.; Comin, R.; Bajdich, M.; Garcia-Melchor, M.; Han, L. L.; Xu, J. X.; Liu, M.; Zheng, L. R.; et al.

Homogeneously Dispersed Multimetal Oxygen-evolving Catalysts. *Science* **2016**, *352*, 333−337.

(41) Nurlaela, E.; Shinagawa, T.; Qureshi, M.; Dhawale, D. S.; Takanabe, K. Temperature Dependence of Electrocatalytic and Photocatalytic Oxygen Evolution Reaction Rates Using NiFe Oxide. *ACS Catal.* **2016**, *6*, 1713−1722.